The embryonic mouse hindbrain and postnatal retina as *in vivo* models to study angiogenesis

Alessandro Fantin[1] and Christiana Ruhrberg [2]

[1] Department of Biosciences, University of Milan, Via G. Celoria 26, 20133, Milan, Italy. Email: alessandro.fantin@unimi.it

[2] UCL Institute of Ophthalmology, University College London, 11-43 Bath Street, London EC1V 9EL.

Summary

Angiogenesis, the growth of new blood vessels from pre-existing ones, is a fundamental process for organ development, exercise-induced muscle growth and wound healing, but is also associated with different diseases such as cancer and neovascular eye disease. Accordingly, elucidating the molecular and cellular mechanisms of angiogenesis has the potential to identify new therapeutic targets to stimulate new vessel formation in ischemic tissues or inhibit pathological vessel growth in disease. This chapter describes the mouse embryo hindbrain and postnatal retina as models to study physiological angiogenesis and provides detailed protocols for tissue dissection, sample staining and analysis.

Key words

Angiogenesis, hindbrain, retina

Running title

Mouse models of physiological angiogenesis

Abbreviations

DABCO (1,4-diazabicyclo[2.2.2]octane)

dpc (days post coitum)

IB4 (isolectin B4)

NRP (neuropilin)

P (postnatal day)

PBS (Phosphate buffered saline)

RT (room temperature)

SVP (subventricular vascular plexus)

SVZ (subventricular zone)

VEGF (vascular endothelial growth factor)

1. Introduction

Angiogenesis is a tightly regulated process involving a range of cell types and signalling pathways, and therefore the choice of the right experimental model is critical to uncover molecular and cellular mechanisms that are of physiological relevance. Many different experimental settings have been exploited, ranging from the simplest *in vitro* models that examine specific parameters implicated in angiogenesis, to complex *in vivo* models that recapitulate key features of pathological conditions with a prominent neovascular component, such as murine models of solid cancers or ischemic eye pathology. Yet, much knowledge of cellular and molecular mechanisms controlling vascular growth and patterning has been provided by studies of vascular growth in developing organs. In particular, several recent studies into the mechanisms of angiogenesis utilised the mouse embryo hindbrain (e.g. [1-11]) and the perinatal mouse retina (e.g. [9-17]).

1.1 The mouse embryo hindbrain

The embryonic central nervous system is vascularised by angiogenic sprouting in a highly stereotypical fashion [1,3,18-21]. Vascularisation of the developing mouse brain starts between 9.5 and 10.0 days post coitum (dpc); during that time, the limiting membrane on the brain surface is degraded focally and capillary sprouts extend radially from the perineural vascular plexus into the neuroectodermal tissue in response to vascular endothelial growth factor (VEGF) A secreted by neuroprogenitors [22-24]. The capillary sprouts consist of solid cords of cells composed of a leading tip cell that extends filopodia and 1 or 2 trailing stalk cells [1, 3, 25].

Next, capillary sprouts elongate towards the ventricular surface, reaching the subventricular zone (SVZ) of the brain with its neuroprogenitors by 10.5 dpc (Fig. 1B). Blood vessel sprouts then change direction by turning approximately 90 degrees to grow laterally. Subsequently, these vessels branch and anastomose with adjacent sprouts to form a vascular plexus that supplies the SVZ and is termed the subventricular vascular plexus (SVP) [1,19,3,20]. Between 10.5 and 12.5 dpc, the SVP can be visualised easily when the roofplate is opened and the hindbrain is flat-mounted and imaged from the dorsal side (Fig. 1A-D) [1, 3, 19, 20].

The main advantage of the hindbrain as a model system for angiogenesis is that growth follows a spatially and temporally well-defined sequence of events [20]. Moreover, the hindbrain can be easily dissected and used for whole-mount immunostaining, ligand binding assays and mRNA in situ hybridisation techniques, with the 2D planar nature of the nascent SVP greatly facilitating imaging of the growing blood vessels [20]. In addition, blood vessel density in the hindbrain can be readily quantified in flatmounts as the number of microvessel branchpoints and intersections

when it is imaged from the ventricular side (Fig. 1A-C,F), or as the number of vessel sprouts that invade the hindbrain from the perineural plexus when it is imaged from the ventral side (Fig. 1E) [1, 3, 19, 20]. Finally, this model system allows the study of mice lacking specific genes implicated in vessel development if they survive the period of vasculogenesis, even if the mutation causes lethality after 12.5 dpc [20]. For example, the hindbrain model has been used to describe angiogenesis defects in mice expressing only the soluble VEGF120 isoform of VEGF-A, but lacking the heparin/neuropilin (NRP) binding VEGF164 isoform; these mice die within the first 2 weeks after birth (Fig. 3A,B) [26]. In addition, the hindbrain analysis allowed the characterisation of mice lacking the VEGF164 receptor NRP1, which die between 10.5 dpc and 14.5 dpc depending on the genetic background [11, 27-29]. In cases where embryonic lethality in constitutive knockout mice occurs prior to hindbrain angiogenesis, modern genetic techniques, such as constitutive or tamoxifen-inducible Cre/lox technology, can be used to allow conditional gene deletion only in selected cell lineages or just prior to hindbrain angiogenesis [30].

1.2 The postnatal mouse retina

Three different types of vascular networks support eye development: choroid, hyaloid and retinal vessels. Whilst the first two networks form during embryogenesis to support eye specification and growth, the retinal vasculature appears only after birth, concomitant with hyaloid vessel regression (reviewed in [31,32]). Retinal vessels emerge from the optic nerve head at the centre of the retina and extend outward to form a two-dimensional planar network, variably called the primary, superficial or inner vascular plexus (Fig. 2); these vessels follow a gradient of VEGF-A deposited by retinal astrocytes that migrate in front of the nascent vasculature [13, 33]. The more

mature vessels near the optic nerve head begin to remodel after postnatal day (P) 3 and form an alternating radial pattern of arteries and veins that are connected by capillary beds. At around P8, the primary vascular plexus has reached the periphery of the retina. Subsequently, vessels start sprouting downwards to form two deeper plexi that will provide oxygen and nutrients to the internal retinal layers. In this process, angiogenic sprouts emerge from veins, venules and capillaries near veins to penetrate the retina. Initially, the vascular sprouts grow perpendicular to the primary plexus along Müller cell processes, but turn laterally when they reach the inner or outer boundary of the inner nuclear layer. In this fashion, they establish the deeper vascular plexus and then the intermediate vascular plexus. By the third week of age, all three networks are fully established in mice [31,32].

Similar to the embryonic hindbrain, an advantage of the developing mouse retina as a model system for angiogenesis is the planar nature of its primary vascular plexus, because it facilitates the visualisation of angiogenic sprouting in flat-mounts. Also similar to the embryonic hindbrain, retinal angiogenesis proceeds in a stereotypical and well-defined sequence of events, as described above. In addition, remodelling in the centre of the primary plexus allows the study of vascular maturation in the same preparation used to study sprouting at the vascular front. Thus, some vessel segments increase in diameter as they remodel into arteries and veins, whilst other vessel segments are pruned to reinforce optimal blood flow in vessels that are retained. Pruning is particularly evident in the vicinity of arteries, where capillary free zones emerge. This process can occur via migration and relocalisation of endothelial cells into feeder vessels or via selective endothelial cell apoptosis [34].

Even though the retina provides a useful model system to study arteriovenous remodeling, this feature also reduces its suitability for quantitative analysis of capillary

branching complexity, as areas containing only capillaries are small and interspersed between arteries and veins (Fig. 2B,C).

The fact that the retinal vasculature develops postnatally can also pose a disadvantage when the targeting of genes implicated in vessel development leads to embryonic lethality (e.g. the *Vegfa*, *Vegfr1*, *Vegfr2* and *Nrp1* genes). However, the development of constitutive or tamoxifen-inducible conditional knock-out technology can overcome this limitation, as for the hindbrain model [30].

As an advantage over the hindbrain model, the retina is more accessible to experimental manipulation, such as the local injection of drugs, inhibitors or growth factors treatments [13]. Furthermore, the postnatal retina can be explanted and cultured for live imaging or *ex vivo* pharmacological treatments [35].

2. Materials

2.1 Equipment

96-well flat-bottom tissue culture plate.

Benchtop centrifuge.

Benchtop orbital shaker.

Benchtop tube roller.

Confocal laser scanning microscope.

Dissection instruments: standard curved forceps, Watchmaker forceps (no. 5 or 55), standard surgical scissors and spring scissors.

Electrical tape.

Epifluorescence stereomicroscope equipped with a digital camera.

Falcon tubes, 50 ml.

Glass bottles.

Glass coverslips, 22 × 55 mm.

Glass slides.

Fibre optic gooseneck lamps.

Parafilm.

Plastic cell culture dishes, 60-mm diameter.

Plastic Pasteur pipettes.

Round-bottomed reagent tubes, 2.0 ml.

Stereomicroscope equipped with a digital camera.

Tabletop balance.

Water bath.

2.2 Reagents

Absolute methanol.

Alexa Fluor 633-conjugated streptavidin (Life Technologies, cat. no. S32354). It is possible to choose an alternative fluorophore-conjugated streptavidin.

Biotinylated IB4 from Bandeiraea simplicifolia BS-I (Sigma, cat. no. L2140).

Blocking solution (0.1% Triton X-100 (v/v) and 10% normal goat serum (v/v) in PBS).

Mowiol/DABCO antifade (0.6% Mowiol 4-88 (w/v) in 25% glycerol with 2.5% DABCO (w/v)).

Paraformaldehyde (PFA); dissolve at 4% (w/v) in PBS to yield formaldehyde fixative.

PBS.

PBT (0.1% Triton X-100 (v/v) in PBS).

Rising methanol gradient (25%, 50% and 75% (vol/vol) absolute methanol in PBS, then absolute methanol).

SlowFade antifade reagent kit (Life Technologies, cat. no. S2828).

3. Methods

3.1 Hindbrain dissection and fixation

To obtain mouse embryos of defined gestational ages, mice are mated in the evening, and the morning of vaginal plug formation is counted as 0.5 dpc. The females are culled at the desired dpc (usually 11.5 dpc for sprouting phase analysis or 12.5 dpc for analysis of the mature SVP) by cervical dislocation and the uterine horns harvested and placed into a plastic dish with ice cold PBS. Under a dissecting stereomicroscope, use forceps to remove each individual embryo sac from the uterus and rupture the yolk sac. Using the forceps, cut the embryo head just above the forearms (Fig. 1A, step 1) and remove the face (Fig. 1A, step 2) [20]. Sever the skin and the pial membrane of the roofplate covering the fourth ventricle in the dorsal side of the head (Fig. 1A, step 3) and continue to cut toward the midbrain (Fig. 1A, step 4) and the spinal cord (Fig. 1A, step 5), allowing the not-yet-fused developing neural tube to unfold. After removal of the head mesenchyme and the pial membrane from the ventral side of the neural tube (Fig. 1A, step 6), separate the midbrain (Fig. 1A, step 7) and beginning of the spinal cord from the unfurled hindbrain (Fig. 1A, step 8) [20].

Using a plastic Pasteur pipette transfer the samples to a 2 ml plastic tube and fix in 1 ml of formaldehyde at 4°C for 2 hours on a benchtop tube roller. Increasing the opening of the pipette by cutting off a portion of the tip will prevent any damage to the unfixed hindbrains. After fixation, wash the hindbrains in PBS and either process them for whole-mount immunostaining or store them for a short term in PBS at 4°C. For storage longer than a few days, it is recommended to dehydrate the hindbrains through a rising methanol gradient to store them at -20°C for up to 3 months [20].

3.2 Retina dissection and fixation

Mouse pups of the desired age (usually between P4 and P7 for primary plexus analysis) are culled by cervical dislocation. The eyes are removed immediately and fixed for 5 minutes in formaldehyde at room temperature (RT) in a plastic dish. The fixative is then replaced with PBS for further dissection. Grab the cornea with the forceps (Fig. 2A, step 1) and cut along the border between the sclera and the iris using spring scissors (Fig. 2A, step 2). After dissecting the cornea, remove the iris (Fig. 2A, step 3) and pull the lens out with the forceps; this action normally also removes any remaining fragments of iris, the ciliary body, the hyaloid vasculature and the vitreous humour (Fig. 2A, step 4). Ensure to completely remove the hyaloid vessels that might still be connected to the optic nerve head region before fixing the retina. Carefully peel the sclera and retinal pigmented epithelium (rpe) away from the retina (Fig. 2A, step 5). To flat-mount the dissected retina, make four radial incisions using spring scissors (Fig. 2A, step 6), position the retina with the inner side facing upward (Fig. 2A) and remove excess PBS from the dish using a plastic Pasteur pipette. If the retina is not completely opened up, flatten the unfolded lobes using curved forceps.

Fix the tissue by slowly dropping cold 100% methanol directly on the centre of the retina for a few seconds until the tissue appears white and stiff. Using curved forceps, transfer the retina to a 96-well plate already containing 200 µl of methanol, seal the plate with parafilm and incubate at -20°C for 2 hours. Retinas can be stored at -20°C for many months, provided that methanol in the wells is replenished regularly, as it evaporates over time even in the freezer.

3.3 Whole-mount staining

For whole-mount staining, the samples are washed in PBS twice at RT. Hindbrains can be pooled into one 2 ml plastic tube (maximal four hindbrains per tube) and processed in a minimum volume of 300 µl in subsequent steps. Retinas are instead transferred with curved forceps into the wells of a fresh 96-well plate previously filled with PBS and should be kept in a volume of 100 µl to cover the sample throughout the staining procedure. During all subsequent incubations, tubes containing hindbrains are placed on a benchtop tube roller, whilst plates containing retinas are placed on an orbital shaker and agitated at the lowest speed available. The samples are permeabilised and blocked against unspecific interactions by incubating for 30 minutes to 1 hour at RT in the blocking solution, and then incubated in the blocking solution containing a 1:200 dilution of biotinylated IB4 overnight at 4ºC (see note 2). Samples are washed 3 times in PBT at RT for 15 minutes each and then incubated overnight at 4ºC or for 2 hours at RT with Alexa-conjugated streptavidin in blocking solution (see notes 2 to 4). Samples are then washed as described above and post-fixed in formaldehyde at 4ºC for at least 30 minutes.

3.4 Imaging

To image the fluorescently labelled hindbrains, two layers of electrical tape are placed on a glass slide, and squares are cut to create pockets large enough to accommodate a single hindbrain [20]. Using a Pasteur pipette, the hindbrains are then transferred to the pockets and, after removing of excess PBS, mounted in SlowFade (Molecular Probes) underneath a coverslip with the ventricular side facing up (see notes 4 and 5). On the contrary, retinas are placed directly on a slide with the inner side facing up using curved forceps and then mounted using Mowiol/DABCO antifade and a coverslip (see notes 4 and 5).

Fluorescent images for the embryonic hindbrains are best recorded in maximal intensity projections of z-stacks performed with a laser scanning confocal microscope (Fig. 1B-E and Fig. 3A,B). High magnification imaging is required to visualize small diameter structures such as tip cells and their filopodia (Fig. 1E). Turning the slide upside down will allow visualization of blood vessels entering the brain from the pial side (Fig. 1F).

Postnatal retinas can be imaged using a fluorescent stereomicroscope at 1.6x magnification to capture the whole retina in a single picture (Fig. 2B and Fig. 3C,D), while confocal imaging is required to obtain more detailed images of the vasculature including tip cell filopodia (Fig. 2C,D).

3.5 Quantitation of angiogenesis

For each hindbrain, the number of vessel intersections or radial vessels can be easily quantified manually in images of the ventricular or pial side, respectively (e.g., Fig.1B,E). For the retina, low magnification images allow the quantification of radial vascular expansion from the centre towards the periphery of the eye by measuring the distance between the optic nerve head in the centre of the retina and the vascular front of each segment of the mounted tissue (red arrow in Fig. 2A). Several freely available or commercial softwares may be used for automated quantitation of these parameters, such as AngioTool (Fig. 1F) [36], ImageJ, Imaris (Bitplane) or Volocity (Improvision).

4. Notes

1. Figure 3 shows an example of angiogenesis defects in a hindbrain and retina with perturbed VEGF-A gradients relative to littermate wild type controls. Here, the mutant phenotype is due to the expression of only the soluble VEGF120 isoform at the

expense of a mixture of VEGF-A isoforms that include VEGF120 as well as the larger, heparin/NRP-binding VEGF-A isoforms. Only the heterozygous mutant retina is shown because the homozygous mutation is lethal at birth in the C57/Bl6 background (see Subheading 1.1).

2. This protocol can be used for immunostaining the hindbrain or retina with many different antibodies, either alone or in combination, and is compatible with histochemical detection methods (e.g. HRP-conjugated streptavidin), provided that endogenous HRP activity is blocked at the beginning of the staining procedure, and the appropriate blocking reagents and secondary antibodies are selected (see, for example, refs. [10,20,37].

3. If fluorescent speckles are seen, the reason could be that the streptavidin forms precipitates. To avoid this, always centrifuge the streptavidin in a refrigerated benchtop centrifuge at top speed before use to remove precipitates.

4. Weak staining might be due to insufficient tissue penetration by IB4 or photobleaching. Increase incubation time, optimize IB4 concentration, keep samples in the dark (e.g. wrap containers in tin foil) and mount samples in antifade solution. The choice of fluorochromes that are excited and emit at high wave lengths (red or far red) will allow improved detection of IB4 in deeper layers of whole-mounted tissues.

5. Trapping of air bubbles in mounted sections can occur when placing the coverslip. Lower the coverslip carefully onto the samples to avoid trapping air bubbles; if bubbles persist, slowly remove the coverslip and repeat the mounting procedure again.

Acknowledgements

We thank Marcus Fruttiger and Shalini Jadeja for teaching us the retina dissection technique. This work was supported by a Medical Research Council grant (MR/N011511/1) to C. Ruhrberg.

References

1. Ruhrberg C, Gerhardt H, Golding M, Watson R, Ioannidou S, Fujisawa H, Betsholtz C, Shima DT (2002) Spatially restricted patterning cues provided by heparin-binding VEGF-A control blood vessel branching morphogenesis. Genes Dev 16(20): 2684–2698

2. Gerhardt H, Ruhrberg C, Abramsson A, Fujisawa H, Shima D, Betsholtz C (2004) Neuropilin-1 is required for endothelial tip cell guidance in the developing central nervous system. Dev Dyn 231(3):503–509

3.Fantin A, Vieira JM, Gestri G, Denti L, Schwarz Q, Prykhozhij S, Peri F, Wilson SW, Ruhrberg C (2010) Tissue macrophages act as cellular chaperones for vascular anastomosis downstream of VEGF-mediated endothelial tip cell induction. Blood 116(5):829–840. https://doi.org/10.1182/blood-2009- 12-257832

4.Fantin A, Vieira JM, Plein A, Denti L, Fruttiger M, Pollard JW, Ruhrberg C (2013) NRP1 acts cell autonomously in endothelium to promote tip cell function during sprouting angiogenesis. Blood 121(12):2352–2362. https://doi.org/10.1182/blood-2012- 05-424713

5. Graupera M, Guillermet-Guibert J, Foukas LC, Phng LK, Cain RJ, Salpekar A, Pearce W, Meek S, Millan J, Cutillas PR, Smith AJ, Ridley AJ, Ruhrberg C, Gerhardt H, Vanhaesebroeck B (2008) Angiogenesis selectively requires the p110alpha isoform of PI3K to control endo- thelial cell migration. Nature 453(7195): 662–666.

https://doi.org/10.1038/ nature06892

6. Lu X, Le Noble F, Yuan L, Jiang Q, De Lafarge B, Sugiyama D, Breant C, Claes F, De Smet F, Thomas JL, Autiero M, Carmeliet P, Tessier-Lavigne M, Eichmann A (2004) The

netrin receptor UNC5B mediates guidance events controlling morphogenesis of the vascu- lar system. Nature 432(7014):179–186

Tammela T, Zarkada G, Nurmi H, Jakobsson L, Heinolainen K, Tvorogov D, Zheng W, Franco CA, Murtomaki A, Aranda E, Miura N, Yla-Herttuala S, Fruttiger M, Makinen T, Eichmann A, Pollard JW, Gerhardt H, Alitalo K (2011) VEGFR-3 controls tip to stalk conversion at vessel fusion sites by reinforcing Notch signalling. Nat Cell Biol 13(10):1202–1213. https://doi.org/10. 1038/ncb2331

Plein A, Fantin A, Denti L, Pollard JW, Ruhr- berg C (2018) Erythro-myeloid progenitors contribute endothelial cells to blood vessels. Nature 562(7726):223–228. https://doi. org/10.1038/s41586-018-0552-x

Fantin A, Herzog B, Mahmoud M, Yamaji M, Plein A, Denti L, Ruhrberg C, Zachary I (2014) Neuropilin 1 (NRP1) hypomorphism combined with defective VEGF-A binding reveals novel roles for NRP1 in developmental and pathological angiogenesis. Development 141(3):556–562. https://doi.org/10.1242/ dev.103028

Fantin A, Schwarz Q, Davidson K, Normando EM, Denti L, Ruhrberg C (2011) The cyto- plasmic domain of neuropilin 1 is dispensable for angiogenesis, but promotes the spatial sep- aration of retinal arteries and veins. Develop- ment 138(19):4185–4191. https://doi.org/ 10.1242/dev.070037

11. Fantin A, Lampropoulou A, Gestri G, Raimondi C, Senatore V, Zachary I,

Ruhrberg C (2015) NRP1 regulates CDC42 activation to promote filopodia formation in endothelial tip cells. Cell Rep 11(10):1577–1590. https://doi.org/10.1016/j.celrep.2015.05.018

Benedito R, Roca C, Sorensen I, Adams S, Gossler A, Fruttiger M, Adams RH (2009) The notch ligands Dll4 and Jagged1 have opposing effects on angiogenesis. Cell 137(6): 1124–1135. https://doi.org/10.1016/j.cell. 2009.03.025

Gerhardt H, Golding M, Fruttiger M, Ruhrberg C, Lundkvist A, Abramsson A, Jeltsch M, Mitchell C, Alitalo K, Shima D, Bet- sholtz C (2003) VEGF guides angiogenic sprouting utilizing endothelial tip cell filopo- dia. J Cell Biol 161(6):1163–1177. https://doi.org/10.1083/jcb.200302047

Wang Y, Nakayama M, Pitulescu ME, Schmidt TS, Bochenek ML, Sakakibara A, Adams S, Davy A, Deutsch U, Luthi U, Barberis A, Ben- jamin LE, Makinen T, Nobes CD, Adams RH (2010) Ephrin-B2 controls VEGF-induced angiogenesis and lymphangiogenesis. Nature

465(7297):483–486. https://doi.org/10.

1038/nature09002

15. Hellstrom M, Phng LK, Hofmann JJ, Wallgard E, Coultas L, Lindblom P, Alva J, Nilsson AK, Karlsson L, Gaiano N, Yoon K, Rossant J, Iruela-Arispe ML, Kalen M, Gerhardt H, Betsholtz C (2007) Dll4 signal- ling through Notch1 regulates formation of tip cells during angiogenesis. Nature 445(7129): 776–780. https://doi.org/10.1038/nature05571

16. Liyanage SE, Fantin A, Villacampa P, Lange CA, Denti L, Cristante E, Smith AJ, Ali RR, Luhmann UF, Bainbridge JW, Ruhrberg C (2016) Myeloid-derived vascular endothelial growth factor and hypoxia-inducible factor are dispensable for ocular neovascularization--brief report. Arterioscler Thromb Vasc Biol 36(1): 19–24.

https://doi.org/10.1161/ ATVBAHA.115.306681

17. Raimondi C, Fantin A, Lampropoulou A, Denti L, Chikh A, Ruhrberg C (2014) Imati- nib inhibits VEGF-independent angiogenesis by targeting neuropilin 1-dependent ABL1 activation in endothelial cells. J Exp Med 211(6):1167–1183. https://doi.org/10. 1084/jem.20132330

18. Bar T (1983) Patterns of vascularization in the developing cerebral cortex. Ciba Found Symp 100:20–36

19. Vieira JM, Schwarz Q, Ruhrberg C (2007) Selective requirements for NRP1 ligands dur- ing neurovascular patterning. Development 134(10):1833–1843. https://doi.org/10. 1242/dev.002402

20. Fantin A, Vieira JM, Plein A, Maden CH, Ruhrberg C (2013) The embryonic mouse hindbrain as a qualitative and quantitative model for studying the molecular and cellular mechanisms of angiogenesis. Nat Protoc 8(2): 418–429. https://doi.org/10.1038/nprot. 2013.015

21. Tata M, Ruhrberg C, Fantin A (2015) Vascu- larisation of the central nervous system. Mech Dev 138(pt 1):26–36. https://doi.org/10. 1016/j.mod.2015.07.001

22. Breier G, Albrecht U, Sterrer S, Risau W (1992) Expression of vascular endothelial growth factor during embryonic angiogenesis and endothelial cell differentiation. Develop- ment 114:521–532

23. Raab S, Beck H, Gaumann A, Yuce A, Gerber HP, Plate K, Hammes HP, Ferrara N, Breier G (2004) Impaired brain angiogenesis and neu- ronal apoptosis induced by conditional homo- zygous inactivation of vascular endothelial growth factor. Thromb Haemost 91(3):

595–605. https://doi.org/10.1160/TH03-

09-0582

Haigh JJ, Morelli PI, Gerhardt H, Haigh K, Tsien J, Damert A, Miquerol L, Muhlner U, Klein R, Ferrara N, Wagner EF, Betsholtz C, Nagy A (2003) Cortical and retinal defects caused by dosage-dependent reductions in VEGF-A paracrine signaling. Dev Biol 262(2):225–241. pii:S0012160603003567

Farrell CL, Risau W (1994) Normal and abnor- mal development of the blood-brain barrier. Microsc Res Tech 27(6):495–506

Carmeliet P, Ng YS, Nuyens D, Theilmeier G, Brusselmans K, Cornelissen I, Ehler E, Kakkar VV, Stalmans I, Mattot V, Perriard JC, Dewerchin M, Flameng W, Nagy A, Lupu F, Moons L, Collen D, D'Amore PA, Shima DT (1999) Impaired myocardial angiogenesis and ischemic cardiomyopathy in mice lacking the vascular endothelial growth factor isoforms VEGF164 and VEGF188. Nat Med 5(5): 495–502

Schwarz Q, Gu C, Fujisawa H, Sabelko K, Gertsenstein M, Nagy A, Taniguchi M, Kolod- kin AL, Ginty DD, Shima DT, Ruhrberg C (2004) Vascular endothelial growth factor con- trols neuronal migration and cooperates with Sema3A to pattern distinct compartments of the facial nerve. Genes Dev 18(22): 2822–2834. https://doi.org/10.1101/gad. 322904

Kawasaki T, Kitsukawa T, Bekku Y, Matsuda Y, Sanbo M, Yagi T, Fujisawa H (1999) A require- ment for neuropilin-1 in embryonic vessel for- mation. Development 126(21):4895–4902

Jones EA, Yuan L, Breant C, Watts RJ, Eich- mann A (2008) Separating genetic and hemo- dynamic defects in neuropilin 1 knockout embryos. Development 135(14):2479–2488. https://doi.org/10.1242/dev.014902

30. Nagy A (2000) Cre recombinase: the universal reagent for genome tailoring. Genesis 26(2): 99–109

31. Fruttiger M (2007) Development of the retinal vasculature. Angiogenesis 10(2):77–88. https://doi.org/10.1007/s10456-007- 9065-1

32. Hofmann JJ, Luisa Iruela-Arispe M (2007) Notch expression patterns in the retina: an eye on receptor-ligand distribution during angio- genesis. Gene Expr Patterns 7(4):461–470. https://doi.org/10.1016/j.modgep.2006. 11.002

33. Carmeliet P, Tessier-Lavigne M (2005) Com- mon mechanisms of nerve and blood vessel wiring. Nature 436(7048):193–200

34. Hughes S, Chang-Ling T (2000) Roles of endothelial cell migration and apoptosis in vas- cular remodeling during development of the central nervous system. Microcirculation 7(5): 317–333

35. Sawamiphak S, Ritter M, Acker-Palmer A (2010) Preparation of retinal explant cultures to study ex vivo tip endothelial cell responses. Nat Protoc 5(10):1659–1665. https://doi. org/10.1038/nprot.2010.130

36. Zudaire E, Gambardella L, Kurcz C, Vermeren S (2011) A computational tool for quantitative analysis of vascular networks. PloS One 6(11): e27385. https://doi.org/10.1371/journal. pone.0027385

37. Pitulescu ME, Schmidt I, Benedito R, Adams RH (2010) Inducible gene targeting in the neonatal vasculature and analysis of retinal angiogenesis in mice. Nat Protoc 5(9): 1518–1534. https://doi.org/10.1038/nprot. 2010.113

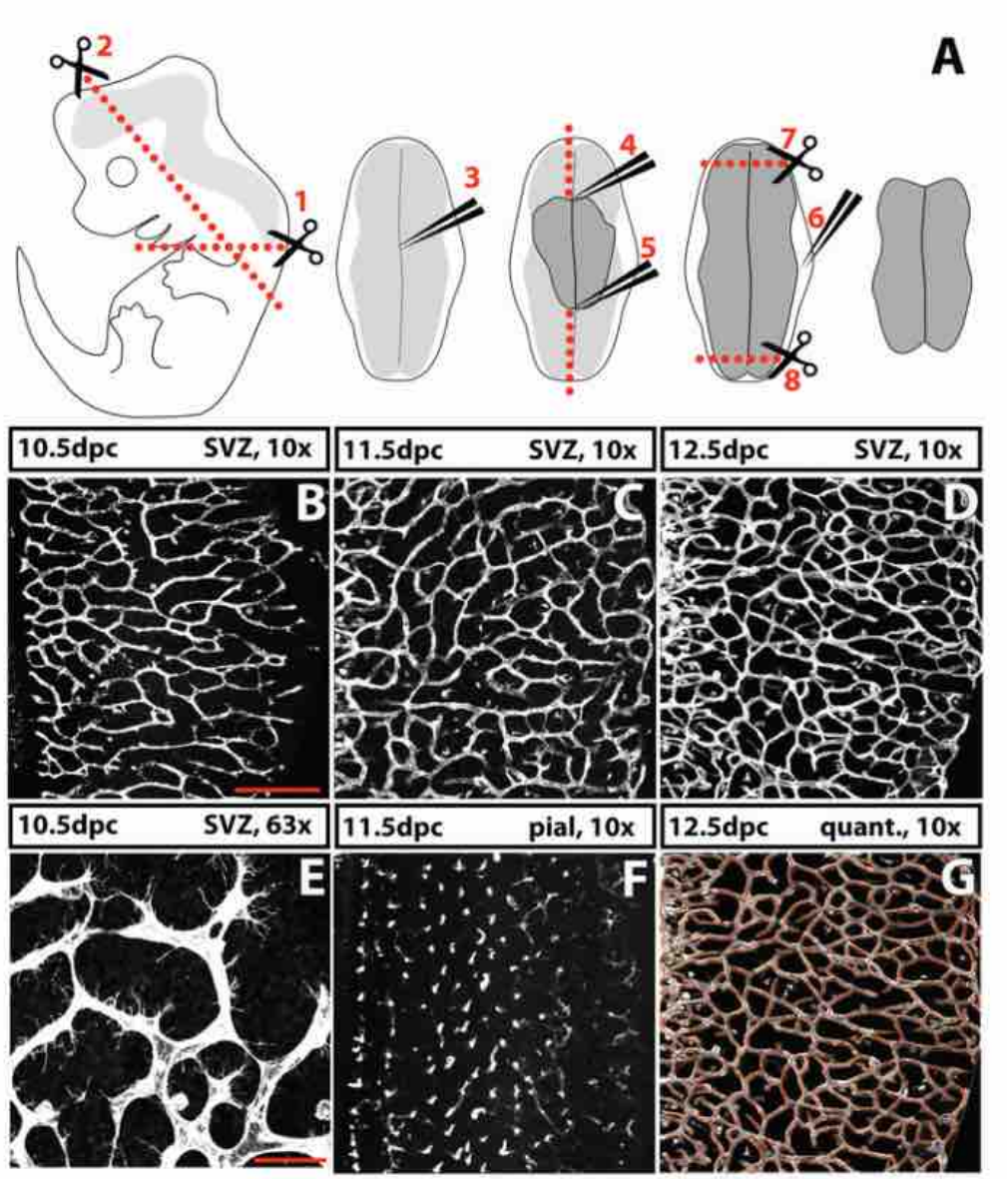

Fig. 1

(a) Schematic of a 12.5 dpc hindbrain dissection. The embryonic brain is shown in gray. Cut the embryo head just above the forearms (step 1) and remove the face (step 2). Sever the skin and the pial membrane of the roof plate covering the fourth ventricle in the dorsal side of the head (step 3) and continue to cut toward the midbrain (step 4) and the spinal cord (step 5), allowing the not-yet-fused developing neural tube to unfold. After removal of the head mesenchyme and the pial membrane from the ventral side of the neural tube (step 6), separate the midbrain (step 7) and beginning of the spinal cord (step 8) from the unfurled hindbrain. (b–g) IB4 staining of the SVZ in 10.5 (b), 11.5 (c), and 12.5 dpc (d) hindbrains using a 10x objective. (e) High magnification image of the SVZ of a 10.5 dpc hindbrain with a 63x objective. (f) IB4 staining of the pial side of a 11.5 dpc hindbrain. (g) Visualization of the vascular intersections (blue dots) by AngioTool in the 12.5 dpc hindbrain shown in (d). Scale bars: 25 μm (b–d, f, g), 50 μm (e)

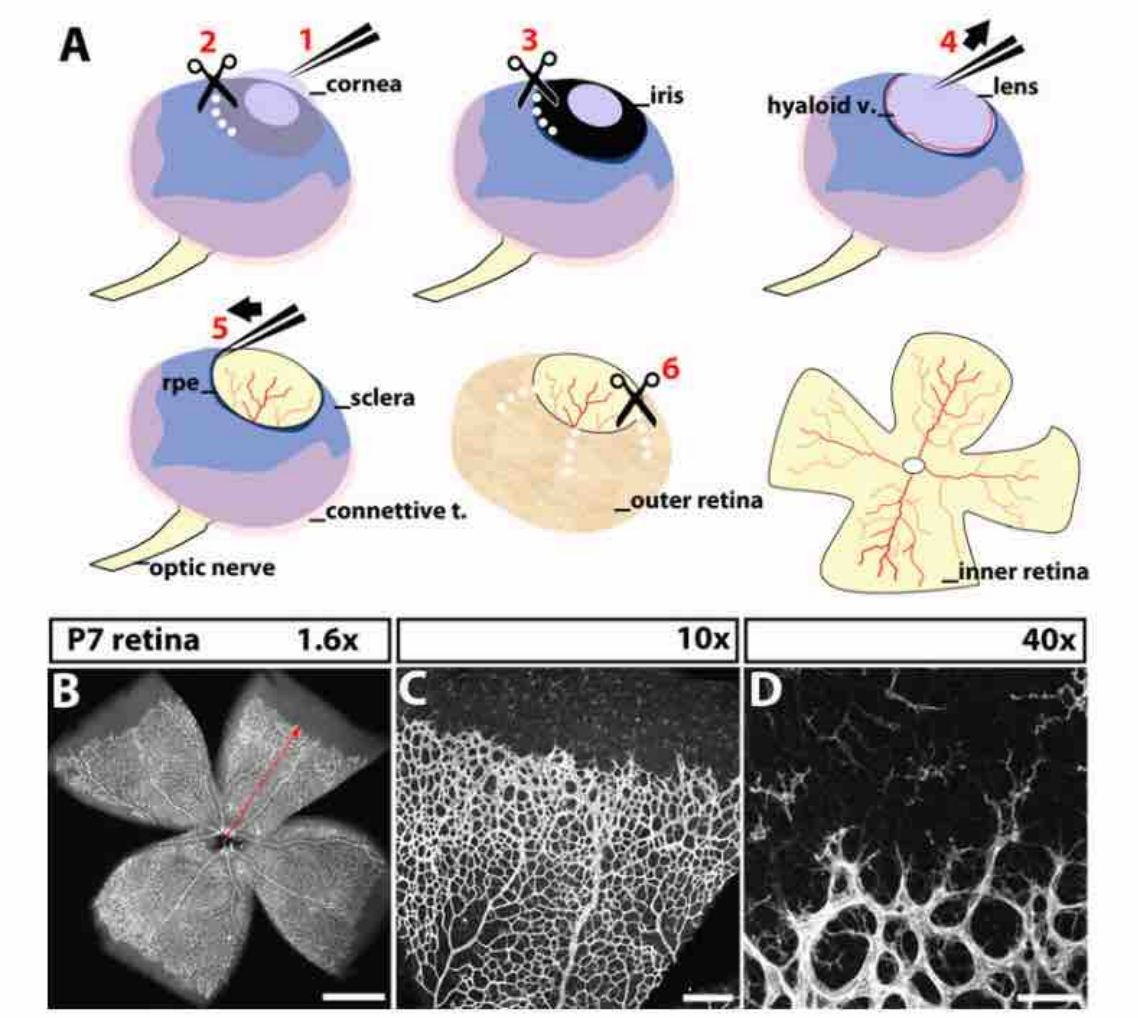

Fig. 2

(a) Schematic of a P7 retina dissection. Grab the cornea with the forceps (step 1) and cut along the border between the sclera and the iris (white dots) using the spring scissors (step 2). After dissecting the cornea, remove the iris (step 3) and pull the lens and the hyaloid vasculature out with the forceps (step 4). Carefully peel away from the retina the outer layers of the eye, which comprise the sclera and the retinal pigmented epithelium (rpe; step 5). Make four radial incisions (step 6) and position the retina with the inner side facing upward. (b) IB4 staining of a P7 retina imaged with a stereomicroscope with 1.6x magnification. (c) Confocal imaging of the same retina shown in (b) with a 10x objective. (d) High magnification imaging of the retina vascular front with a 40x objective. Scale bars: 1 mm (b), 200 μm (c), 50 μm (d)

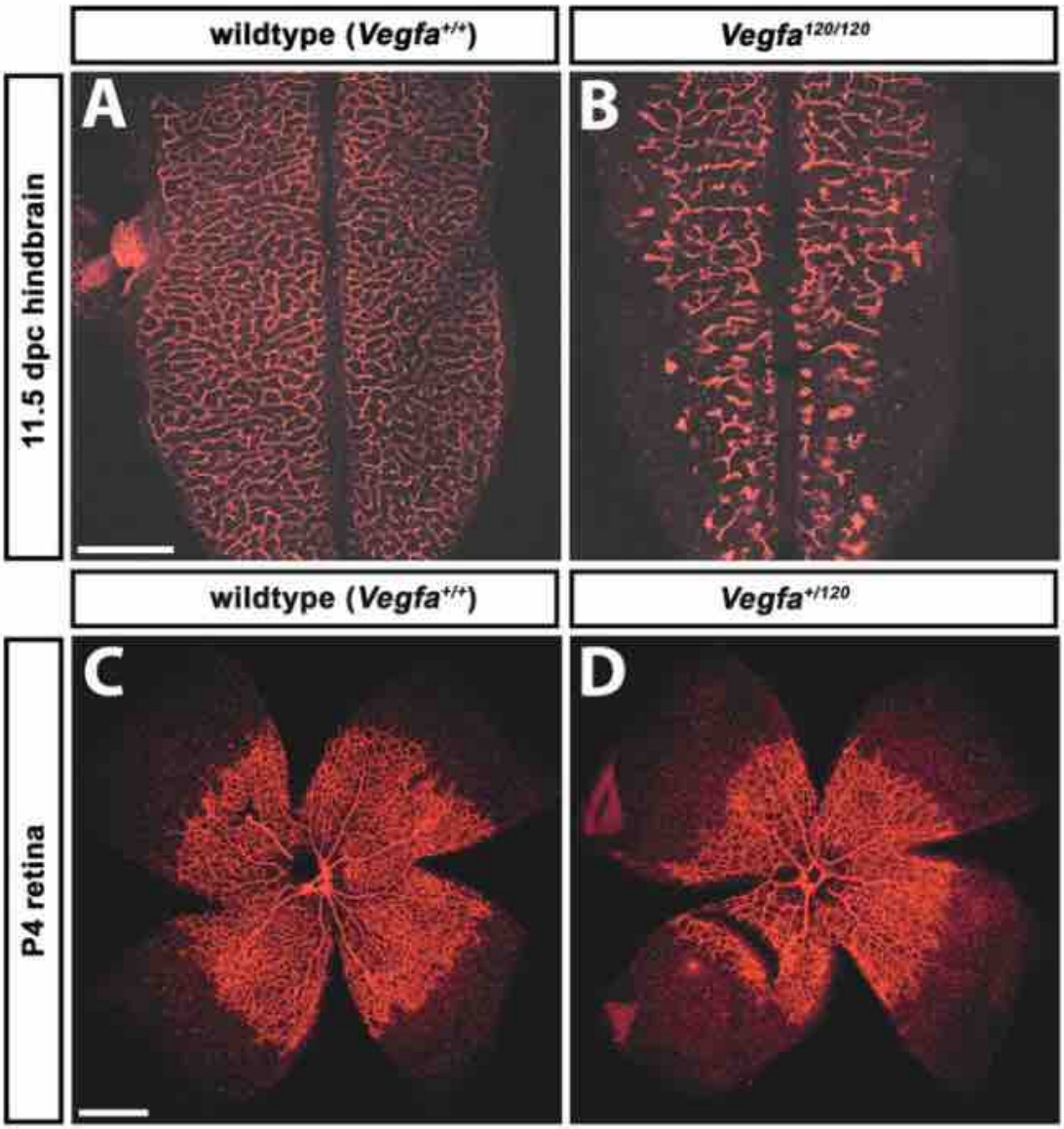

Fig. 3

(a, b) IB4 staining of a *Vegfa*$^{120/120}$ homozygous mutant (b) and littermate control (a) hindbrain at 11.5 dpc. (c, d) IB4 staining of a *Vegfa*$^{+/120}$ heterozygous mutant (d; see Note 1) and littermate control (c) retina at P4. Scale bars: 500 μm (a, b), 1 mm (c, d)